

A multi-axis MEMS sensor with integrated carbon nanotube-based piezoresistors for nanonewton level force metrology

This article has been downloaded from IOPscience. Please scroll down to see the full text article.

2012 Nanotechnology 23 325501

(<http://iopscience.iop.org/0957-4484/23/32/325501>)

View [the table of contents for this issue](#), or go to the [journal homepage](#) for more

Download details:

IP Address: 129.6.32.24

The article was downloaded on 24/09/2012 at 22:21

Please note that [terms and conditions apply](#).

A multi-axis MEMS sensor with integrated carbon nanotube-based piezoresistors for nanonewton level force metrology

Michael A Cullinan^{1,2}, Robert M Panas¹ and Martin L Culpepper¹

¹ Massachusetts Institute of Technology, Department of Mechanical Engineering, Cambridge, MA 02139, USA

² National Institute of Standards and Technology, Intelligent Systems Division, Gaithersburg, MD 20899, USA

E-mail: Culpepper@mit.edu

Received 3 April 2012, in final form 23 May 2012

Published 23 July 2012

Online at stacks.iop.org/Nano/23/325501

Abstract

This paper presents the design and fabrication of a multi-axis microelectromechanical system (MEMS) force sensor with integrated carbon nanotube (CNT)-based piezoresistive sensors. Through the use of proper CNT selection and sensor fabrication techniques, the performance of the CNT-based MEMS force sensor was increased by approximately two orders of magnitude as compared to current CNT-based sensor systems. The range and resolution of the force sensor were determined as 84 μN and 5.6 nN, respectively. The accuracy of the force sensor was measured to be better than 1% over the device's full range.

(Some figures may appear in colour only in the online journal)

1. Introduction

Nanonewton level, multi-axis force sensing is required for many biology, materials science and nanomanufacturing applications. For example, multi-axis, precision force sensing is needed to measure adhesion forces (nNs to μN) between cells and various types of surfaces. These measurements enable one to know (i) how well cells bond to different types of biomedical implant materials and (ii) the effects that drug coatings have on the prevention/promotion of adhesion. This type of measurement is necessary in applications where the mechanical properties of the cell-implant interface are critical [1]. For example, measurements of cell adhesion strength will allow researchers to determine the suitability of different types of materials for the development of biomedical implants. These measurements will allow researchers to determine what materials to use both for areas where cell growth is desired and for areas where there should be no cell growth.

Unfortunately, the requirements of these applications are difficult to achieve given the size, sensitivity and fabrication limitations associated with existing small-scale sensing techniques. Carbon nanotube-based strain sensors have the potential to overcome some of the limitations in small-scale force/displacement sensing technologies due to their small size and high strain sensitivity [2]. In this paper, we will show how carbon nanotube (CNT) based piezoresistive sensors may be used to improve the resolution of multi-axis MEMS sensor systems.

2. Background

MEMS force sensors tend to rely on one of three sensing methods: capacitive sensing, optical laser detection, and piezoresistive sensing. Several multi-axis force sensors have been developed using capacitive sensors [3, 4]. These sensors are difficult to fabricate and require relatively large sensor areas (mm^2) for each axis in order to achieve high force

resolution. This makes capacitive sensing impractical for small, inexpensive, multi-axis force sensors. Optical sensors are widely used in atomic force microscopy (AFM) to make high resolution force measurements in one axis. Optical sensors are rarely used in micro-scale, multi-axis sensing due to the difficulty and cost of integrating multiple sets of optics into a small region. Also, optical sensors require relatively large lasers (10 cm² [5] to 100 cm² [6] footprint) which make it impossible to miniaturize the force sensing system to the micro-scale. Piezoresistive sensors offer the most promise at the micro-scale due to their small size and relative ease of integration into MEMS devices. Piezoresistive transducers are commonly found in MEMS devices such as pressure sensors, accelerometers, and AFM cantilevers [7]. Several dual-axis MEMS cantilevers with nN-level resolution have previously been demonstrated [8, 9].

Most MEMS piezoresistive sensors use either doped single-crystal silicon or poly-crystalline silicon as the piezoresistive element. Single-crystal silicon is attractive for piezoresistive sensors due to its high gauge factor (up to 200 [10]). However, the sensitivity of single-crystal silicon sensors is highly dependent on crystallographic orientation [11]. Therefore, single-crystal silicon cannot be used effectively in multi-axis MEMS sensors, such as the force sensor presented in this paper, where the sensors are in different crystal planes. Polysilicon piezoresistive sensors do not have a directional sensitivity but they have significantly lower gauge factors (up to 30 [10]) than single-crystal silicon sensors. CNT-based piezoresistive sensors fabricated as presented in this paper have gauge factors of 75 ± 5 (standard deviation) [12] which is significantly greater than the typical gauge factors for polysilicon. CNT-based piezoresistors also do not suffer from the directional dependence associated with single-crystal silicon sensors. Therefore, CNT-based piezoresistors are capable of outperforming silicon sensors in multi-axis MEMS sensors [13] and were selected as the sensing element for the device presented in this paper.

Several prototype devices have been fabricated using CNTs as strain sensors. The most common devices use films of randomly oriented films of CNTs as the sensing element. These films are popular due to their ease of fabrication and large size. These properties allow CNT-based film sensors to be integrated into many macroscale sensor systems [14–17]. Overall, these CNT-based piezoresistive films tend to show good linearity (within a few per cent) but generally have low gauge factors (5–10) due to the random orientation of the CNTs in the films and the poor transmittance of the strain in the substrate to the CNTs in the films [15, 18].

There have also been several devices fabricated using individual or a small number of CNTs as the sensing elements. For example, single CNT piezoresistive sensors have been used to measure the force applied to meso-scale beams [12, 19–22] and the strain applied to flexible substrates [23, 24]. In these devices strain is applied to the CNTs through the bending or stretching of the substrate. In addition, MEMS devices such as pressure sensors have also been fabricated using CNT piezoresistors as the sensing element [25]. These CNT-based pressure sensors are capable of pressure resolutions of about 1 psi.

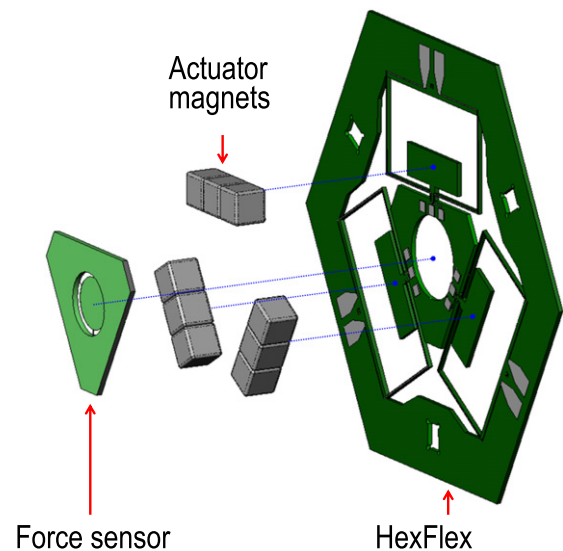


Figure 1. Exploded view of Hexflex–force sensor assembly.

Force and displacement sensors have also been fabricated by suspending individual CNTs between electrodes and attaching a beam to the center of the CNT [26]. When the beam is deflected, the CNT is stretched, causing the resistance to change. Such devices are capable of sub-nanonewton force resolution. Unfortunately, such single CNT sensors tend to suffer high flicker noise due to their low carrier concentration. This means that these single CNT devices tend to be limited to dynamic ranges of less than 40 dB [27]. This is important in flexure based systems since range can be traded for resolution by changing the flexure geometry but the ratio of range to resolution known as the dynamic range is a fixed quantity. Therefore, in order to maximize the performance of flexure based sensor systems it is necessary to maximize the dynamic range.

In order to decrease the flicker noise and overcome this dynamic range limitation, the multi-axis force sensor presented in this paper is designed with multiple CNTs arranged in a parallel resistor network. This parallel network resistor configuration reduces the total noise in the sensor by increasing the charge carrier concentration while allowing a high sensor gauge factor to be maintained by limiting the number of tube–tube junctions in the electrical path.

3. Force sensor design

The multi-axis force sensor presented in this paper is designed to fit on top of a Hexflex nanopositioner as seen in figure 1 [28].

In this setup, the HexFlex nanopositioner is used to precisely move the multi-axis force sensor. The precise, six degree-of-freedom motion of the HexFlex is necessary to properly position the force sensor into place and align the center stage of the force sensor with the surface of the cells. The HexFlex can then be used to lower the force sensor stage into contact with the cells and to make sure uniform pressure is applied over the entire cell array. After the cells bond to

Table 1. Force sensor functional requirements.

Functional requirement	Value
Measurement axis	Z, θ_x, θ_y
Range	100s of μN
Resolution	$\sim 1 \text{ nN}$
Natural frequency	1 kHz
Cost	$< \$100$
Footprint	$< 1 \text{ mm}^2$

the center stage of the force sensor, the HexFlex can be used to slowly retract the force sensor from the surface to which the cells are adhered. Using feedback from the force sensor, the HexFlex can be used to compensate for any torques that might be applied to the cells during this retraction phase and to ensure that only the direct force normal to the cell surface is being measured. Overall, this setup and procedure makes it possible to accurately and precisely quantify the adhesion forces between cells and different types of surfaces.

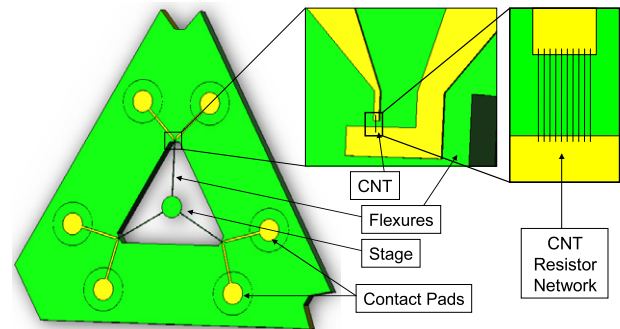
3.1. Functional requirements

Accurate measurement of cell adhesion forces between surfaces requires multi-axis sensing to make sure that the surfaces are suitably positioned and oriented, thereby ensuring that load is applied evenly over the surfaces during testing. Cellular adhesion forces are typically on the scale of nN's [29]. When thousands of cells are arrayed on the surface being tested, the adhesion force is on the order of 100s of μN . Therefore, to be useful, the force sensor must have 100s of μN range and nN-level resolution. The natural frequency of the force sensor was set to 1 kHz in order to ensure that it was capable of operating at least 1 order of magnitude faster than the HexFlex, which has a natural frequency of $\sim 100 \text{ Hz}$. This ensures that the force sensor can be used in feedback mode with the HexFlex, even when the HexFlex is operating at its maximum speed.

The force sensor must also be capable of measuring forces perpendicular to the plane of contact (Z) and torques about axes that are parallel to the planes of contact, (θ_x, θ_y). This is to ensure that the force sensor is applying an uniform force over the entire cell array. In addition, the force sensor must fit on the central stage of the Hexflex and must have a low cost ($< \$100$) so that it can be replaced after each test. These functional requirements are summarized in table 1.

3.2. CNT-based force sensor design

A comprehensive system level noise model was used to design the CNT-based force sensor [30]. The force sensor is comprised of three coplanar flexures with integrated CNT-based piezoresistive sensors at the base of the flexures. The piezoresistive sensors consist of 100s of CNTs are stretched between electrodes spaced $1 \mu\text{m}$ apart. This design allows each of the CNTs to be strained and minimizes the CNT–CNT interactions which can reduce the sensitivity of CNT-based piezoresistive films. In addition, this design helps to reduce the flicker noise in the sensor by increasing the

**Figure 2.** Three-axis force sensor with CNT-based piezoresistors.**Table 2.** CNT-based force sensor design.

Property	Value
Beam length	2.5 mm
Beam width	$35 \mu\text{m}$
Beam thickness	$10 \mu\text{m}$
Maximum force	$100 \mu\text{N}$
Natural frequency	1 kHz
Dynamic range	83 dB

carrier concentration of the sensor. Therefore, through the use of this type of design architecture it is possible to increase the resolution of CNT-based MEMS sensors by almost two orders of magnitude over current designs [27].

The CNT-based piezoresistors are arranged into a quarter Wheatstone bridge. A full Wheatstone bridge was not used due to fabrication and thermal heating constraints. The CNT-based piezoresistors are connected to aluminum contact pads on the outer base of the force sensor via aluminum traces. The sensors are placed at the base of the structure to maximize the strain imposed upon the resistors. A schematic of the CNT-based piezoresistive force sensor is given in figure 2.

The final flexure dimensions of the force sensor are a beam length of 2.5 mm, a beam width of $35 \mu\text{m}$ and a beam thickness of $10 \mu\text{m}$. Based on this design it was estimated that the CNT-based piezoresistive force sensor should have a force range of approximately $100 \mu\text{N}$ and a resolution of approximately 7 nN. This works out to a dynamic range of 83 dB based on previous modeling of the sensor system [13]. In addition, the estimated natural frequency was approximately 1000 Hz. These design properties are presented in table 2.

4. Force sensor fabrication

The CNT-based MEMS force sensors were fabricated using a combination of conventional microfabrication and self-assembly techniques [31]. The MEMS force sensors were fabricated using conventional microfabrication techniques, as described in figure 3. The process starts with a 150 mm silicon-on-insulator (SOI) wafer with a $10 \mu\text{m}$ device layer, a $500 \mu\text{m}$ handle layer, and a $1 \mu\text{m}$ oxide layer. First, an RCA clean is used to remove any contaminants from the wafer surface. The wafer is then placed in the oxide furnace and 300 nm of thermal oxide is grown on the wafer. The

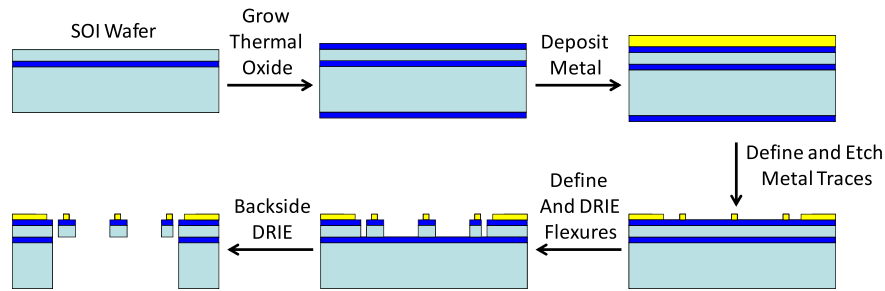


Figure 3. Three-axis force sensor with CNT-based piezoresistors.

thermal oxide acts as an electrical insulating layer between the piezoresistive sensors and the device structure. Next, the wafer is placed in the low-pressure chemical vapor deposition (LPCVD) furnace and 500 nm of polysilicon is grown on the wafer. This polysilicon is used as the piezoresistive material for half of the force sensors on the wafer. The rest of the force sensors are left blank so that CNT-based piezoresistors can be deposited after the microfabrication process is complete. After the polysilicon is deposited it is placed in an annealing furnace to improve the resistivity of the polysilicon and to ensure that the dopants are evenly distributed throughout the film.

After these high temperature processing steps are completed, a protective photoresist coating is applied to the front side of the wafer and the back side polysilicon is removed. Next photolithography is used to define the pattern of the polysilicon on the wafer and reactive ion etching is used to remove the polysilicon from the unwanted areas. After the polysilicon piezoresistors are defined, the wafer is cleaned using an ashers to remove the photoresist and a piranha clean to remove any other contaminates, before 500 nm of aluminum is sputtered onto the wafer. Again, photolithography is used to define the wire traces and bond pads while etching is used to remove the excess aluminum from the wafer.

Next, a protective photoresist is applied to the front side of the wafer so that it is not damaged while a buffered oxide etch (BOE) is used to remove the thermal oxide from the back side of the wafer. After this step, photolithography is used to define the flexure structure on the front side of the wafer. A BOE is used to remove the oxide from the front side of the wafer and deep reactive ion etching (DRIE) is used to create the flexures in the handle layer. The ashers is used to remove excess photoresist from the front side of the wafer.

Finally, the front side of the wafer is then mounted to a quartz handle wafer and photolithography is used to pattern the back side of the wafer. The handle wafer acts as both a protective layer for the front side as well as a mechanical structure that holds the wafer together after the DRIE step. DRIE is used to etch the back side of the wafer and to release the flexures from the handle layer of the SOI wafer. DRIE is also used to etch through the entire wafer in order to separate the wafer into devices. After the DRIE step, a vapor hydrofluoric acid (HF) step is used to remove the excess oxide from the insulating layer of the SOI wafer and the wafer is placed into an acetone bath to separate the chips from the quartz wafer. In finally, a laser ablation system is used to separate any chips that may still be attached to each other.

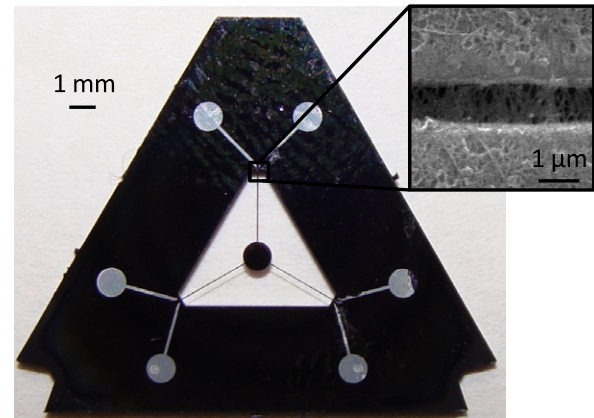


Figure 4. Fabricated 3-axis force sensor with CNT-based piezoresistors. Inset shows CNTs between the two electrodes.

After the microfabrication is complete, CNT-based piezoresistors are deposited onto the blank CNT force sensors using dielectrophoresis. A droplet of a 3 g l^{-1} CNT solution is placed on the gap between the electrodes on the force sensor structure. A 5 V peak-to-peak ac voltage with a frequency of 5 MHz is used to align the CNTs between the two electrodes. This deposition process is continued for 15 min in order to ensure that the maximum number of CNTs are deposited on the force sensor structure. After the sensors are deposited by dielectrophoresis, they are coated in an aluminum oxide protective layer and annealed at 525°C for 30 min in order to minimize the amount of noise in the sensor. The final result of this fabrication process is shown in figure 4.

5. Device stiffness

The stiffness of the force sensor was measured using the Hysitron TriboIndenter. In order to do this, the force sensor was mounted in a test plate and the nanoindenter was used to deflect the center stage of the force sensor. An array of points on the center stage was indented on the center stage in order to find the center of stiffness. By measuring the load–displacement curve at each of the indentation locations it is possible to determine the vertical and torsional stiffnesses of the force sensor. Using this method it is possible to get an accurate measurement of the force sensor stiffness. The measured stiffness versus the distance from the centroid of the force sensor is shown in figure 5. From these measurements

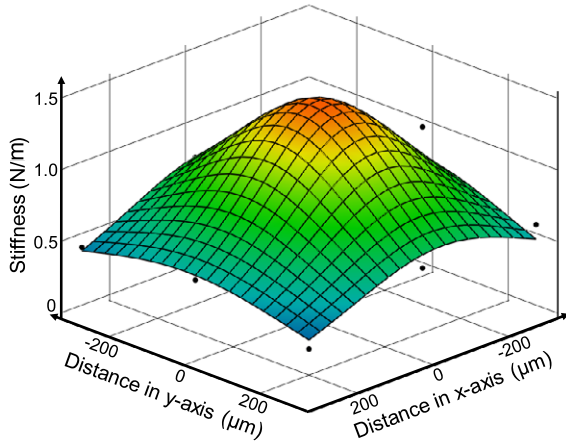


Figure 5. Measured force sensor stiffness as a function of the distance from the centroid of the force sensor in the x and y -axes.

the vertical stiffness of the force sensor was determined to be 1.4 N m^{-1} and the torsional stiffnesses around the x and y -axes were 150 nN m and 110 nN m , respectively.

6. Calibration

In order to calibrate the force sensor, a specialized calibration setup was built to relate the force applied to the central stage of the force sensor to the output of each of the piezoresistive sensors as shown in figure 6. This specialized setup was required since the electronics and electrical probes necessary to measure the output of the piezoresistive sensors could not be fit into the limited space inside the chamber of the nanoindenter. In this setup, the force sensor is calibrated by using a micrometer to actuate the center stage of the force sensor. The micrometer has a digital readout with a resolution of $1 \mu\text{m}$. Spring pins are used to connect the bond pads on the force sensor to wires that run to the Wheatstone bridge circuit. These spring pins provide a preload to the force sensor to hold it in place during testing and ensure that all of the bond pads are in contact during testing. A 1 mm diameter stainless steel ball is connected to the tip of the micrometer head in order to ensure a small contact area and to prevent torques from being transmitted to the center stage from the rotation of the micrometer head.

In order to calibrate the force sensor, the readout from each of the sensors was amplified through the Wheatstone bridge circuit and read into Labview. An initial measurement for all three sensors was taken, then the micrometer was actuated by $1 \mu\text{m}$ and a new set of measurements was recorded. This process was continued for $35 \mu\text{m}$ or until the force sensor reached about $1/3$ of its predicted maximum displacement. The output of each sensor was recorded for each $1 \mu\text{m}$ displacement. Using the measured stiffness of the force sensor, these displacement measurements were converted into force measurements. These measurements were then used to create calibration curves for each piezoresistor in the force sensor and determine the force sensitivity of each of the piezoresistors. The experimental error in these force measurements was about $\pm 1.4 \mu\text{N}$ due to

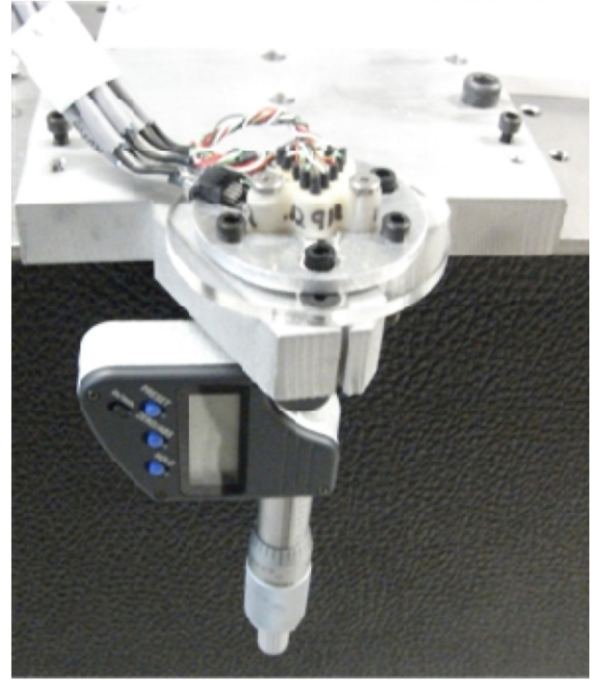


Figure 6. Force sensor calibration setup.

the uncertainty in the magnitude and position of the measured displacements as well as the uncertainty in the measured stiffness of the force sensor.

7. Force and torque calculations

When a force or a torque is applied to the central stage of the force sensor, the beams connecting the central stage to the base of the MEMS device deflect and strain the piezoresistors. This strain in the piezoresistors changes the resistance of the piezoresistors and creates a voltage output reading from the Wheatstone bridge circuit. These output voltages can be used to calculate the forces and torques on each of the individual piezoresistive sensors using the calibration constants determined for each sensor. Therefore, the forces and the torques on the central stage of the force sensor can be calculated from a linear combination of the output voltages from each of the sensors. Similarly, the displacement of the central stage can be calculated by multiplying the calculated forces on the stage by the compliance of the stage. The forces and torques on the central stage of the force sensor are given by equations (1)–(3) where F_z is the out of plane force, T_{θ_x} is the torque about the x -axis, T_{θ_y} is the torque about the y -axis, V is the voltage output, S is the force sensitivity in Volts per Newton, L is the distance between the force location and the sensor location, and θ is angle between the force location and the sensor location with respect to the y -axis.

$$F_z = \frac{V_1}{S_1} + \frac{V_2}{S_2} + \frac{V_3}{S_3} \quad (1)$$

$$T_{\theta_x} = \cos(\theta_1) \frac{V_1}{S_1} L_1 + \cos(\theta_2) \frac{V_2}{S_2} L_2 + \cos(\theta_3) \frac{V_3}{S_3} L_3 \quad (2)$$

$$T_{\theta_y} = \sin(\theta_1) \frac{V_1}{S_1} L_1 + \sin(\theta_2) \frac{V_2}{S_2} L_2 + \sin(\theta_3) \frac{V_3}{S_3} L_3. \quad (3)$$

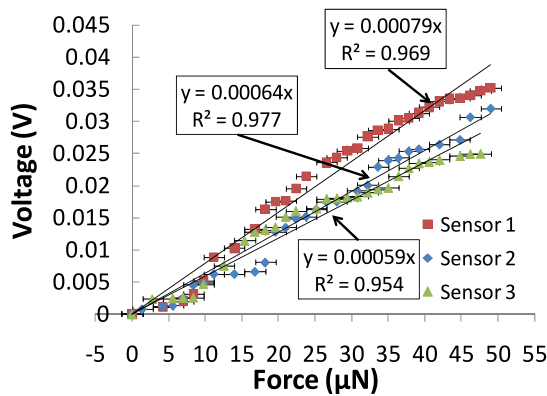


Figure 7. Calibration curve for each CNT-based sensor on the force sensor.

For the force sensor presented in this paper with a force applied at the center of the stage, θ_1 is 0° , θ_2 is 120° and θ_3 is 240° .

8. Results

Overall, the measured force sensitivity varies by about 25% between the sensors. Sensor 1 has a sensitivity of $0.79 \text{ mV } \mu\text{N}^{-1}$, while sensors 2 and 3 have sensitivities of $0.64 \text{ mV } \mu\text{N}^{-1}$ and $0.59 \text{ mV } \mu\text{N}^{-1}$ respectively. Each of these calibration curves explains over 95% of the variance in voltage with the increase in force applied to the structure. Therefore, the uncertainty in the force calibration is low and the measured uncertainty of the slope of the calibration line or accuracy for the force sensor of better than 1% over the device's full range. The calibration results for each sensor are presented in figure 7.

In addition to the linear calibration curves, each sensor appears to have a sinusoidal component. This component is likely due to thermal variations over the testing period. The thermal coefficient of resistance (TCR) of the CNT-based piezoresistive sensors was measured to be approximately $0.27\% \text{ K}^{-1}$ which is consistent with previously measured TCRs for CNT-based thin films [32–34]. The overall measured sensor drift is consistent with this TCR measurement given the $\pm 1^\circ \text{C}$ variance in room temperature over the measurement period. The total test took about 20 min, which is approximately equal to the thermal period of the room. Therefore, we would expect to see about 1 full thermal period in each sensor due to thermal variations of the room. These thermal variations account for the majority of the drift in the sensor.

The differences in force sensitivities between the three sensors could be due to either the differences in the gauge factors of the sensors or to asymmetric loading of the structure by the micrometer. Previous results with the test structures have shown that the gauge factor of CNT-based piezoresistive sensors can vary by up to 12% (95% confidence interval) due to variations in the composition of the CNTs in the sensor [12]. This explains about half of the variation between the sensors.

The measured gauge factors for each of the CNT-based piezoresistive sensors in the MEMS force sensor range from 62 to 83 with an average value of about 71. Previous results for CNT-based strain sensors fabricated using the method described in the paper had an average value of 75 with a standard deviation of 5 [12]. Therefore, the gauge factor results for the CNT-based piezoresistors in the force sensor are consistent with previous results and all fall within the 99% confidence interval of the previously measured sensors. The increased variance in the CNT-based piezoresistive sensors presented in this paper versus previous results could be due to the fact that the piezoresistive sensors on the MEMS force sensor are an order of magnitude smaller than the previously tested structures. Therefore, fewer CNTs contribute to overall gauge factor of the sensor causing the variance between the sensors to increase.

Asymmetric loading of the force sensor by the micrometer could also contribute to the difference in measured sensitivities by imposing torques onto the force sensor as well as z -axis displacement. These torques would cause some of the flexure beams to be strained more than others, which would result in the higher readouts from these sensors. For example, a positive torque around the x -axis would result in an increased strain on sensor 1 but a decreased strain on sensors 2 and 3. Such a torque could be created if the location of the actuation was moved in the positive y -direction from the center of stiffness of the force sensor. Such an offset could either be created by small fabrication errors that result in the center of stiffness not being at the same location as the geometric center or by the actuator not pushing directly on the geometric center of the force sensor. Either way, this type of torque about the x -axis could help explain the remaining discrepancy between the measured sensitivities of each of the sensors. Eventually, it should be possible to compensate for this type of asymmetric loading by incorporating feedback control between the HexFlex nanopositioner and the force sensor stage.

The total range of the system was measured by increasing the displacement of the micrometer head until a sharp change in the sensor readout was observed. This sharp change was caused by the fracture of one of the flexure beams, which caused the readout from the sensor on that flexure beam to return to its original value, since the strain on the CNT-based piezoresistors decreased to zero. Overall, the range of the sensor was measured to be about $60 \mu\text{m}$. The stiffness of the force sensor measured from the nanoindentation tests was 1.4 N m^{-1} . Therefore the force range of the force sensor was measured to be $84 \mu\text{N}$.

The resolution of each sensor was calculated by dividing the noise in each sensor by the sensitivity of each sensor. The measured resolution for sensor 1 was 9.5 nN and it was 11.8 nN and 6.7 nN for sensors 2 and 3, respectively. The results for each sensor along with the corresponding measured dynamic ranges for each sensor are presented in table 3.

The overall resolution of the force sensor is calculated by taking the weighted sum of squares of each of the three sensors in the force sensor structure [35]. Based on this calculation, the resolution of the force sensor is approximately

Table 3. Results for each piezoresistor in the force sensor.

	Sensor 1	Sensor 2	Sensor 3
Sensitivity (V N^{-1})	790	640	590
Noise (μV)	7.5	7.5	4.0
Gauge factor	83	67	62
Force resolution (nN)	9.5	11.8	6.7
Strain resolution	6.5×10^{-8}	8.0×10^{-8}	4.6×10^{-8}
Dynamic range (dB)	78.4	76.5	81.3

5.6 nN. This corresponds to a dynamic range of 83 dB and matches the predicted dynamic range for the sensor of 83.2 dB with less than 0.25% error. This dynamic range is an improvement of more than two orders of magnitude over the dynamic range previously reported for other CNT-based piezoresistive sensor systems [27].

9. Conclusions

The dynamic range of the force sensor presented in this paper compares favorably with other multi-axis MEMS sensors which are typically larger and operate at lower speeds than the device presented in this paper. For example, several two degree-of-freedom, x - y stages have been designed with capacitive sensors [36, 37]. These stages have similar dynamic ranges as the sensor presented in this paper but have sensor footprints that several orders of magnitude larger than the sensors presented in this paper. In addition, capacitive force sensors that have been fabricated with more than two degrees-of-freedom typically have dynamic ranges that are an order of magnitude lower than the force sensors presented in this paper [3].

Polysilicon-based multi-axis piezoresistive sensors typically have a dynamic range that is an order of magnitude lower than the force sensor presented in this paper [38]. This is due to the fact that polysilicon has a lower strain sensitivity than the CNT-based sensors presented in this paper. For example, a similar multi-axis force sensor with the CNT-based piezoresistive sensors replaced by polysilicon piezoresistors only has a dynamic range of 57 dB [38].

From these results, it is clear that the dynamic range of multi-axis MEMS sensors can be significantly improved through the use of carbon nanotube-based piezoresistors. However, more work still needs to be done in order to maximize the dynamic range of these sensors. Further improvements in the performance of the CNT-based can be achieved using the design optimization procedures described in [13] and the manufacturing optimization procedures described in [39]. For example, the dynamic range of the force sensor can be improved by redesigning the force sensor system to increase the sensor area. Also, the force sensor could be improved by incorporating higher gauge factor CNTs into the sensor through the use of CNT sorting [40]. Overall, these changes could help to increase the dynamic range of the force sensor to over 110 dB. Therefore, the force sensor could achieve a resolution of about 100 pN while maintaining the same range as the current CNT-based force sensor.

References

- [1] Xue W, Krishna B V, Bandyopadhyay A and Bose S 2007 Processing and biocompatibility evaluation of laser processed porous titanium *Acta Biomater.* **3** 1007–18
- [2] Stampfer C, Jungen A, Linderman R, Obergefell D, Roth S and Hierold C 2006 Nano-electromechanical displacement sensing based on single-walled carbon nanotubes *Nano Lett.* **6** 1449–53
- [3] Beyeler F, Muntwyler S, Nelson B J and Member S 2009 A six-axis MEMS force–torque sensor with micro-Newton and nano-newtonmeter resolution *J. Microelectromech. Syst.* **18** 433–41
- [4] Sun Y and Nelson B J 2007 MEMS capacitive force sensors for cellular and flight biomechanics *Biomed. Mater.* **2** S16–22
- [5] Jager G *et al* 2003 Miniature interferometers for applications in microtechnology and nanotechnology *Proc. SPIE* **5190** 185–92
- [6] Zhang Z and Menq C-H 2007 Laser interferometric system for six-axis motion measurement no title *Rev. Sci. Instrum.* **78** 083107
- [7] Tortonese M, Barrett R C and Quate C F 1993 Atomic resolution with an atomic force microscope piezoresistive detection *Appl. Phys. Lett.* **62** 834–6
- [8] Chui B, Kenny T, Mamin H, Terris B and Rugar D 1998 Independent detection of vertical and lateral forces with a sidewall-implanted dual-axis piezoresistive cantilever *Appl. Phys. Lett.* **72** 1388–90
- [9] Duc T C, Creemer J and Sarro P M 2007 Piezoresistive cantilever beam for force sensing in two dimensions *IEEE Sensors J.* **7** 96–104
- [10] Beeby S, Ensell G, Kraft M and White N 2004 *MEMS Mechanical Sensors* 1st edn (Norwood, MA: Artchen House) p 88
- [11] Kanda Y 1982 A graphical representation of piezoresistance coefficients in silicon *IEEE Trans. Electron Dev.* **29** 64–70
- [12] Cullinan M and Culpepper M 2010 Carbon nanotubes as piezoresistive microelectromechanical sensors: theory and experiment *Phys. Rev. B* **82** 115482
- [13] Panas R M, Cullinan M A and Culpepper M L 2012 Design of piezoresistive-based MEMS sensor systems for precision microsystems *Precis. Eng.* **36** 44–54
- [14] Xue W and Cui T 2008 Electrical and electromechanical characteristics of self-assembled carbon nanotube thin films on flexible substrates *Sensors Actuators A* **145/146** 330–5
- [15] Li Z, Dharap P, Nagarajaiah S, Barrera E V and Kim J 2004 Carbon nanotube film sensors *Adv. Mater.* **16** 640–3
- [16] Li X, Levy C and Elaadil L 2008 Multiwalled carbon nanotube film for strain sensing *Nanotechnology* **19** 045501
- [17] Vemuru S M, Wahi R, Nagarajaiah S and Ajayan P M 2009 Strain sensing using a multiwalled carbon nanotube film *J. Strain Anal. Eng. Des.* **44** 555–62
- [18] Dharap P, Li Z, Nagarajaiah S and Barrera E 2004 Nanotube film based on single-wall carbon nanotubes for strain sensing *Nanotechnology* **15** 379–82
- [19] Tong J and Sun Y 2007 Toward carbon nanotube-based AFM cantilevers *IEEE Trans. Nanotechnol.* **6** 519–23
- [20] Yang X, Zhou Z, Zheng F, Zhang M, Zhang J and Yao Y 2009 A high sensitivity single-walled carbon-nanotube-array-based strain sensor for weighing *Solid-State Sensors, Actuators and Microsystems Conf., 2009* pp 1493–6
- [21] Xie Y and Tabib-Azar M 2006 Telescoping self-aligned metal-catalyzed carbon nanotube piezoresistors as strain gauges *IEEE Sensors 2006* pp 1407–10

- [22] Dohn S, Kjelstruphansen J, Madsen D, Molhave K and Boggild P 2005 Multi-walled carbon nanotubes integrated in microcantilevers for application of tensile strain *Ultramicroscopy* **105** 209–14
- [23] Chang N-K, Su C-C and Chang S-H 2008 Fabrication of single-walled carbon nanotube flexible strain sensors with high sensitivity *Appl. Phys. Lett.* **92** 063501
- [24] Maune H and Bockrath M 2006 Elastomeric carbon nanotube circuits for local strain sensing *Appl. Phys. Lett.* **89** 173131
- [25] Stampfer C, Helbling T, Oberfell D, Schöberle B, Tripp M K, Jungen A, Roth S, Bright V M and Hierold C 2006 Fabrication of single-walled carbon-nanotube-based pressure sensors *Nano Lett.* **6** 233–7
- [26] Stampfer C, Jungen A and Hierold C 2006 Fabrication of discrete nanoscaled force sensors based on single-walled carbon nanotubes *IEEE Sensors J.* **6** 613–7
- [27] Helbling T, Roman C and Hierold C 2010 Signal-to-noise ratio in carbon nanotube electromechanical piezoresistive sensors *Nano Lett.* **10** 3350–4
- [28] DiBiasio C M and Culpepper M L 2009 Design of a six degree of freedom nanopositioner for use in massively parallel probe-based nanomanufacturing *Proc. 2009 Annual Mtg of the Am. Soc. for Precision Eng.*
- [29] Van Vliet K 2003 The biomechanics toolbox: experimental approaches for living cells and biomolecules *Acta Mater.* **51** 5881–905
- [30] Panas R M, Cullinan M A and Culpepper M L 2010 A systems approach to modeling of piezoresistive MEMS sensors *Proc. 2010 Am. Soc. for Precision Eng., Control of Precision Systems Conf.*
- [31] Cullinan M A 2011 *Design and Fabrication of Precision Carbon Nanotube-Based Flexural Transducers* (Cambridge, MA: Massachusetts Institute of Technology)
- [32] Itkis M E, Borondics F, Yu A and Haddon R C 2006 Bolometric infrared photoresponse of suspended single-walled carbon nanotube films *Science* **312** 413–6
- [33] Lu R, Xu G and Wu J Z 2011 Effects of thermal annealing on noise property and temperature coefficient of resistance of single-walled carbon nanotube films *Appl. Phys. Lett.* **93** 213101
- [34] Koechlin C, Maine S, Haidar R, Trétout B, Loiseau A and Pelouard J 2010 Electrical characterization of devices based on carbon nanotube films *Appl. Phys. Lett.* **96** 103501
- [35] Cullinan M A, Panas R M and Culpepper M L 2009 Design of micro-scale multi-axis force sensors for precision applications *Proc. 2009 Am. Soc. for Precision Eng.*
- [36] Sun Y, Nelson B, Potasek D and Enikov E 2002 A bulk microfabricated multi-axis capacitive cellular force sensor using transverse comb drives *J. Micromech. Microeng.* **12** 832–40
- [37] Lee J-I, Huang X and Chu P B 2009 Nanoprecision MEMS capacitive sensor for linear and rotational positioning *J. Microelectromech. Syst.* **18** 660–70
- [38] DiBiasio C M 2010 *Concept Synthesis and Design Optimization of Meso-scale, Multi-Degree-of-Freedom Precision Flexure Motion Systems with Integrated Strain-based Sensors* (Cambridge, MA: Massachusetts Institute of Technology)
- [39] Cullinan M A and Culpepper M L 2010 Noise mitigation techniques for carbon nanotube-based piezoresistive sensor systems *Proc. 2010 Fall Mtg of the Materials Research Society*
- [40] Cullinan M A and Culpepper M L 2011 Design and fabrication of single chirality carbon nanotube-based sensors *11th IEEE Conf. Nanotechnology* pp 5–8